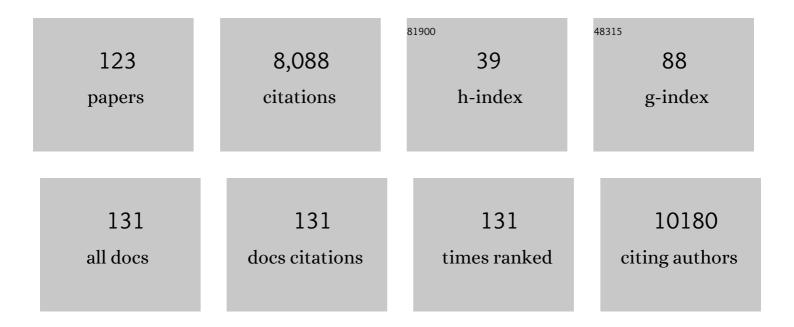
List of Publications by Year in descending order

Source: https://exaly.com/author-pdf/2670112/publications.pdf Version: 2024-02-01



LIANMING RAL

#	Article	IF	CITATIONS
1	Atomic packing and short-to-medium-range order in metallic glasses. Nature, 2006, 439, 419-425.	27.8	1,758
2	A zero-strain layered metal oxide as the negative electrode for long-life sodium-ion batteries. Nature Communications, 2013, 4, 2365.	12.8	515
3	Amorphous Hierarchical Porous GeO _{<i>x</i>} as High-Capacity Anodes for Li Ion Batteries with Very Long Cycling Life. Journal of the American Chemical Society, 2011, 133, 20692-20695.	13.7	288
4	Promotion of water-mediated carbon removal by nanostructured barium oxide/nickel interfaces in solid oxide fuel cells. Nature Communications, 2011, 2, 357.	12.8	280
5	Investigation of structural and electronic properties of graphene oxide. Applied Physics Letters, 2011, 99, .	3.3	252
6	Direct visualization of the Jahn–Teller effect coupled to Na ordering in Na5/8MnO2. Nature Materials, 2014, 13, 586-592.	27.5	237
7	Anomalous Pseudocapacitive Behavior of a Nanostructured, Mixed-Valent Manganese Oxide Film for Electrical Energy Storage. Nano Letters, 2012, 12, 3483-3490.	9.1	234
8	Icosahedral Short-Range Order in Amorphous Alloys. Physical Review Letters, 2004, 92, 145502.	7.8	216
9	A Size-Dependent Sodium Storage Mechanism in Li ₄ Ti ₅ O ₁₂ Investigated by a Novel Characterization Technique Combining in Situ X-ray Diffraction and Chemical Sodiation. Nano Letters, 2013, 13, 4721-4727.	9.1	212
10	In Situ Probing and Synthetic Control of Cationic Ordering in Niâ€Rich Layered Oxide Cathodes. Advanced Energy Materials, 2017, 7, 1601266.	19.5	200
11	Lithium-Doping Stabilized High-Performance P2–Na _{0.66} Li _{0.18} Fe _{0.12} Mn _{0.7} O ₂ Cathode for Sodium Ion Batteries. Journal of the American Chemical Society, 2019, 141, 6680-6689.	13.7	187
12	Microbial synthesis and the characterization of metal-substituted magnetites. Solid State Communications, 2001, 118, 529-534.	1.9	168
13	High energy-density and reversibility of iron fluoride cathode enabled via an intercalation-extrusion reaction. Nature Communications, 2018, 9, 2324.	12.8	136
14	TiS2 as a high performance potassium ion battery cathode in ether-based electrolyte. Energy Storage Materials, 2018, 12, 216-222.	18.0	129
15	The interplay between thermodynamics and kinetics in the solid-state synthesis of layered oxides. Nature Materials, 2020, 19, 1088-1095.	27.5	129
16	Synthetic Control of Kinetic Reaction Pathway and Cationic Ordering in Highâ€Ni Layered Oxide Cathodes. Advanced Materials, 2017, 29, 1606715.	21.0	127
17	Cationic Ordering Coupled to Reconstruction of Basic Building Units during Synthesis of High-Ni Layered Oxides. Journal of the American Chemical Society, 2018, 140, 12484-12492.	13.7	113
18	Highâ€Rate Charging Induced Intermediate Phases and Structural Changes of Layerâ€&tructured Cathode for Lithiumâ€Ion Batteries. Advanced Energy Materials, 2016, 6, 1600597.	19.5	110

JIANMING BAI

#	Article	IF	CITATIONS
19	Overpotential-Dependent Phase Transformation Pathways in Lithium Iron Phosphate Battery Electrodes. Chemistry of Materials, 2010, 22, 5845-5855.	6.7	109
20	What is the Role of Nb in Nickel-Rich Layered Oxide Cathodes for Lithium-Ion Batteries?. ACS Energy Letters, 0, , 1377-1382.	17.4	107
21	Electrochemical decomposition of Li2CO3 in NiO–Li2CO3 nanocomposite thin film and powder electrodes. Journal of Power Sources, 2012, 218, 113-118.	7.8	93
22	Insights into Li/Ni ordering and surface reconstruction during synthesis of Ni-rich layered oxides. Journal of Materials Chemistry A, 2019, 7, 513-519.	10.3	92
23	Nanospheres of a New Intermetallic FeSn ₅ Phase: Synthesis, Magnetic Properties and Anode Performance in Li-ion Batteries. Journal of the American Chemical Society, 2011, 133, 11213-11219.	13.7	88
24	Intrinsic Role of Cationic Substitution in Tuning Li/Ni Mixing in High-Ni Layered Oxides. Chemistry of Materials, 2019, 31, 2731-2740.	6.7	85
25	Phase transition behavior of NaCrO2 during sodium extraction studied by synchrotron-based X-ray diffraction and absorption spectroscopy. Journal of Materials Chemistry A, 2013, 1, 11130.	10.3	84
26	Kinetic Limitations in Single rystal Highâ€Nickel Cathodes. Angewandte Chemie - International Edition, 2021, 60, 17350-17355.	13.8	84
27	In Situ XRD Studies of ZnO/GaN Mixtures at High Pressure and High Temperature: Synthesis of Zn-Rich (Ga _{1â^'<i>x</i>} Zn _{<i>x</i>})(N _{1â^'<i>x</i>} O _{<i>x</i>}) Photocatalysts. Journal of Physical Chemistry C, 2010, 114, 1809-1814.	3.1	71
28	Visible Light-Driven H ₂ Production over Highly Dispersed Ruthenia on Rutile TiO ₂ Nanorods. ACS Catalysis, 2016, 6, 407-417.	11.2	71
29	lonic Conduction in Cubic Na ₃ TiP ₃ O ₉ N, a Secondary Na-Ion Battery Cathode with Extremely Low Volume Change. Chemistry of Materials, 2014, 26, 3295-3305.	6.7	68
30	Investigation of the structural changes in Li1â°'xFePO4 upon charging by synchrotron radiation techniques. Journal of Materials Chemistry, 2011, 21, 11406.	6.7	64
31	Explore the Effects of Microstructural Defects on Voltage Fade of Li- and Mn-Rich Cathodes. Nano Letters, 2016, 16, 5999-6007.	9.1	64
32	Elucidation of the surface characteristics and electrochemistry of high-performance LiNiO ₂ . Chemical Communications, 2016, 52, 4239-4242.	4.1	62
33	In Situ Hydrothermal Synthesis of LiFePO ₄ Studied by Synchrotron X-ray Diffraction. Journal of Physical Chemistry Letters, 2011, 2, 1874-1878.	4.6	60
34	Quantification of Honeycomb Number-Type Stacking Faults: Application to Na ₃ Ni ₂ BiO ₆ Cathodes for Na-Ion Batteries. Inorganic Chemistry, 2016, 55, 8478-8492.	4.0	51
35	Structure Tracking Aided Design and Synthesis of Li ₃ V ₂ (PO ₄) ₃ Nanocrystals as High-Power Cathodes for Lithium Ion Batteries. Chemistry of Materials, 2015, 27, 5712-5718.	6.7	50
36	Localized concentration reversal of lithium during intercalation into nanoparticles. Science Advances, 2018, 4, eaao2608.	10.3	50

#	Article	IF	CITATIONS
37	In situ X-ray absorption and diffraction studies of carbon coated LiFe1/4Mn1/4Co1/4Ni1/4PO4 cathode during first charge. Electrochemistry Communications, 2009, 11, 913-916.	4.7	49
38	A lithiation/delithiation mechanism of monodispersed MSn ₅ (M = Fe, Co and FeCo) nanospheres. Journal of Materials Chemistry A, 2015, 3, 7170-7178.	10.3	47
39	<i>In Situ</i> Diffraction Study of the Highâ€Temperature Decomposition of <i>t′</i> â€Zirconia. Journal of the American Ceramic Society, 2015, 98, 247-254.	3.8	42
40	Synergistic effect from coaxially integrated CNTs@MoS2/MoO2 composite enables fast and stable lithium storage. Journal of Energy Chemistry, 2021, 55, 449-458.	12.9	42
41	Boosting energy efficiency of Li-rich layered oxide cathodes by tuning oxygen redox kinetics and reversibility. Energy Storage Materials, 2021, 35, 388-399.	18.0	42
42	Microanalysis of alkali-activated fly ash–CH pastes. Cement and Concrete Research, 2002, 32, 963-972.	11.0	41
43	Unraveling Na and F coupling effects in stabilizing Li, Mn-rich layered oxide cathodes via local ordering modification. Energy Storage Materials, 2020, 31, 459-469.	18.0	41
44	On the origin of enhanced thermoelectricity in Fe doped Ca3Co4O9. Journal of Materials Chemistry C, 2013, 1, 4114.	5.5	39
45	Characterization of the Fe-Doped Mixed-Valent Tunnel Structure Manganese Oxide KOMS-2. Journal of Physical Chemistry C, 2011, 115, 21610-21619.	3.1	38
46	A new in situ synchrotron X-ray diffraction technique to study the chemical delithiation of LiFePO4. Chemical Communications, 2011, 47, 7170.	4.1	36
47	pH-Dependent Appearance of Chiral Structure in a Langmuir Monolayer. Journal of Physical Chemistry B, 2000, 104, 5797-5802.	2.6	34
48	Cooling Induced Surface Reconstruction during Synthesis of Highâ€Ni Layered Oxides. Advanced Energy Materials, 2019, 9, 1901915.	19.5	34
49	Kinetic Pathways Templated by Low-Temperature Intermediates during Solid-State Synthesis of Layered Oxides. Chemistry of Materials, 2020, 32, 9906-9913.	6.7	34
50	Backbone orientational order in fatty acid monolayers at the air-water interface. Physical Review E, 1998, 58, 7686-7690.	2.1	32
51	1.3†V superwide potential window sponsored by Na-Mn-O plates as cathodes towards aqueous rechargeable sodium-ion batteries. Chemical Engineering Journal, 2019, 370, 742-748.	12.7	32
52	Hydrogen-Bonding Interactions in Hybrid Aqueous/Nonaqueous Electrolytes Enable Low-Cost and Long-Lifespan Sodium-Ion Storage. ACS Applied Materials & Interfaces, 2020, 12, 22862-22872.	8.0	32
53	CoSn5 Phase: Crystal Structure Resolving and Stable High Capacity as Anodes for Li Ion Batteries. Journal of Physical Chemistry Letters, 2012, 3, 1488-1492.	4.6	31
54	Solvothermal Synthesis of LiMn _{1–<i>x</i>} Fe _{<i>x</i>} PO ₄ Cathode Materials: A Study of Reaction Mechanisms by Time-Resolved in Situ Synchrotron X-ray Diffraction. Journal of Physical Chemistry C, 2015, 119, 2266-2276.	3.1	29

#	Article	IF	CITATIONS
55	Improvement of Li-S battery electrochemical performance with 2D TiS2 additive. Electrochimica Acta, 2018, 292, 779-788.	5.2	29
56	Effect of Headgroup Dissociation on the Structure of Langmuir Monolayers. Langmuir, 2000, 16, 1239-1242.	3.5	28
57	Electrochemical Behavior of Electrolytic Manganese Dioxide in Aqueous KOH and LiOH Solutions: A Comparative Study. Journal of the Electrochemical Society, 2016, 163, A356-A363.	2.9	28
58	<i>In Situ</i> Tracking Kinetic Pathways of Li ⁺ /Na ⁺ Substitution during Ion-Exchange Synthesis of Li _{<i>x</i>} Na _{1.5–<i>x</i>} VOPO ₄ F _{0.5} . Journal of the American Chemical Society, 2017, 139, 12504-12516.	13.7	28
59	Synthesis and Structure of Perovskite ScMnO ₃ . Inorganic Chemistry, 2013, 52, 9692-9697.	4.0	27
60	A structural change in Ca ₃ Co ₄ O ₉ associated with enhanced thermoelectric properties. Journal of Physics Condensed Matter, 2012, 24, 455602.	1.8	26
61	Thermal behavior of polyhalite: a high-temperature synchrotron XRD study. Physics and Chemistry of Minerals, 2017, 44, 125-135.	0.8	26
62	Interplay between two-phase and solid solution reactions in high voltage spinel cathode material for lithium ion batteries. Journal of Power Sources, 2013, 242, 736-741.	7.8	24
63	Residual stress characterization of Al/SiC nanoscale multilayers using X-ray synchrotron radiation. Thin Solid Films, 2010, 519, 759-765.	1.8	23
64	High-Temperature Thermodynamics of Cerium Silicates, A-Ce ₂ Si ₂ O ₇ , and Ce _{4.67} (SiO ₄) ₃ O. ACS Earth and Space Chemistry, 2020, 4, 2129-2143.	2.7	23
65	<i>Operando</i> structural and chemical evolutions of TiS ₂ in Na-ion batteries. Journal of Materials Chemistry A, 2020, 8, 12339-12350.	10.3	23
66	High-temperature oxidation of advanced FeCrNi alloy in steam environments. Applied Surface Science, 2017, 426, 562-571.	6.1	21
67	In-situ dehydration studies of fully K-, Rb-, and Cs-exchanged natrolites. American Mineralogist, 2011, 96, 393-401.	1.9	20
68	<i>In Situ</i> Neutron Diffraction Studies of the Ion Exchange Synthesis Mechanism of Li ₂ Mg ₂ P ₃ O ₉ N: Evidence for a Hidden Phase Transition. Journal of the American Chemical Society, 2017, 139, 9192-9202.	13.7	19
69	Operando Multi-modal Synchrotron Investigation for Structural and Chemical Evolution of Cupric Sulfide (CuS) Additive in Li-S battery. Scientific Reports, 2017, 7, 12976.	3.3	18
70	The Role of Water and Hydroxyl Groups in the Structures of Stetindite and Coffinite, MSiO ₄ (M = Ce, U). Inorganic Chemistry, 2021, 60, 718-735.	4.0	18
71	Crossover of thermal expansion from positive to negative by removing the excess fluorines in cubic ReO ₃ -type TiZrF _{7â^'x} . Journal of Materials Chemistry C, 2018, 6, 5148-5152.	5.5	17
72	Grazing incidence X-ray diffraction studies on the structures of polyurethane films and their effects on adhesion to Al substrates. Polymer, 2003, 44, 6663-6674.	3.8	16

#	Article	IF	CITATIONS
73	NaAlTi3O8, A Novel Anode Material for Sodium Ion Battery. Scientific Reports, 2017, 7, 162.	3.3	16
74	Conditioning the Surface and Bulk of High-Nickel Cathodes with a Nb Coating: An <i>In Situ</i> X-ray Study. Journal of Physical Chemistry Letters, 2021, 12, 7908-7913.	4.6	16
75	Layer Ordering and Faulting in(GaAs)n/(AlAs)nUltrashort-Period Superlattices. Physical Review Letters, 2003, 91, 106103.	7.8	15
76	Guiding Synthesis of Polymorphs of Materials Using Nanometric Phase Diagrams. Journal of the American Chemical Society, 2018, 140, 17290-17296.	13.7	15
77	Revealing Reaction Pathways of Collective Substituted Iron Fluoride Electrode for Lithium Ion Batteries. ACS Nano, 2020, 14, 10276-10283.	14.6	14
78	Ultrafast solid-liquid intercalation enabled by targeted microwave energy delivery. Science Advances, 2020, 6, .	10.3	12
79	Two Length Scales and Crossover Behavior in the Critical Diffuse Scattering fromV2H. Physical Review Letters, 1998, 81, 2276-2279.	7.8	11
80	Anomalous-X-ray scattering associated with short-range order in an Al70Ni15Co15 decagonal quasicrystal. Materials Science & Engineering A: Structural Materials: Properties, Microstructure and Processing, 2000, 294-296, 299-302.	5.6	11
81	X-ray diffraction from CuPt-ordered III-V ternary semiconductor alloy films. Physical Review B, 2001, 63, .	3.2	11
82	Assessment of a synchrotron X-ray method for quantitative analysis of calcium hydroxide. Cement and Concrete Research, 2003, 33, 1553-1559.	11.0	11
83	Atomic scattering factor for a spherical wave and near-field effects in x-ray fluorescence holography. Physical Review B, 2003, 68, .	3.2	11
84	lsotropic Low Thermal Expansion over a Wide Temperature Range in Ti1–xZrxF3+x (0.1 ≤ ≤0.5) Solid Solutions. Inorganic Chemistry, 2018, 57, 14396-14400.	4.0	11
85	<i>In situ</i> synchrotron pair distribution function analysis to monitor synthetic pathways under electromagnetic excitation. Journal of Materials Chemistry A, 2020, 8, 15909-15918.	10.3	11
86	Synthesis and Processing by Design of Highâ€Nickel Cathode Materials. Batteries and Supercaps, 2022, 5, .	4.7	11
87	Ambient synthesis, characterization, and electrochemical activity of LiFePO4 nanomaterials derived from iron phosphate intermediates. Nano Research, 2015, 8, 2573-2594.	10.4	10
88	Li ₁₅ P ₄ S ₁₆ Cl ₃ , a Lithium Chlorothiophosphate as a Solid-State Ionic Conductor. Inorganic Chemistry, 2020, 59, 226-234.	4.0	9
89	Design nanoporous metal thin films <i>via</i> solid state interfacial dealloying. Nanoscale, 2021, 13, 17725-17736.	5.6	9
90	Combined computational and experimental investigation of the La ₂ CuO _{4– <i>x</i> } S _{<i>x</i>} (0 ≤i>x ≤) quaternary system. Proceedings of the National Academy of Sciences of the United States of America, 2018, 115, 7890-7895.	7.1	8

#	Article	lF	CITATIONS
91	Enhanced Formation of Solvent-Shared Ion Pairs in Aqueous Calcium Perchlorate Solution toward Saturated Concentration or Deep Supercooling Temperature and Its Effects on the Water Structure. Journal of Physical Chemistry B, 2019, 123, 9654-9667.	2.6	8
92	Atomic-scale structural and chemical evolution of Li3V2(PO4)3 cathode cycled at high voltage window. Nano Research, 2019, 12, 1675-1681.	10.4	8
93	3D Morphology of Bimodal Porous Copper with Nano-Sized and Micron-Sized Pores to Enhance Transport Properties for Functional Applications. ACS Applied Nano Materials, 2020, 3, 7524-7534.	5.0	8
94	Probing Kinetics of Water-in-Salt Aqueous Batteries with Thick Porous Electrodes. ACS Central Science, 2021, 7, 1676-1687.	11.3	8
95	Structural studies of NH4-exchanged natrolites at ambient conditions and high temperature. American Mineralogist, 2011, 96, 1308-1315.	1.9	7
96	The Effect of Silver Ion Occupancy on Hollandite Lattice Structure. MRS Advances, 2018, 3, 547-552.	0.9	6
97	Anion and cation co-doping of Na4SnS4 as sodium superionic conductors. Materials Today Physics, 2020, 15, 100281.	6.0	6
98	Change from a bulk discontinuous phase transition in V2H to a continuous transition in a defective near-surface skin layer. Modelling and Simulation in Materials Science and Engineering, 2000, 8, 269-275.	2.0	5
99	Determination of the order parameter of CuPt-Bordered GaInP2 films by x-ray diffraction. Journal of Applied Physics, 2002, 91, 9039-9042.	2.5	5
100	Structural, magnetic, and transport studies of La0.8MnO3 films. Journal of Applied Physics, 2002, 92, 4518-4523.	2.5	5
101	Structural studies of annealed ultrathin La0.8MnO3 films. Applied Physics Letters, 2002, 80, 2663-2665.	3.3	5
102	Influence of strain on the atomic and electronic structure of manganite films. Journal of Physics and Chemistry of Solids, 2007, 68, 458-463.	4.0	5
103	Residual Stress Analysis of Boronized AISI 1018 Steel by Synchrotron Radiation. Journal of Materials Engineering and Performance, 2008, 17, 730-732.	2.5	5
104	Adhesion of a rigid polyurethane foam to zinc phosphated steel. Journal of Adhesion Science and Technology, 2003, 17, 1351-1368.	2.6	4
105	Chemical and Hydrostatic Pressure in Natrolites: Pressure-Induced Hydration of an Aluminogermanate Natrolite. Journal of Physical Chemistry C, 2010, 114, 18805-18811.	3.1	4
106	Multi-Modal Synchrotron Characterization: Modern Techniques and Data Analysis. , 2020, , 39-64.		4
107	Increased performance with 12-mrad sagittal-focusing monochromator. AIP Conference Proceedings, 2000, , .	0.4	3
108	X-ray study of antiphase boundaries in the quadruple-period ordered GaAs0.87Sb0.13 alloy. Journal of Applied Physics, 2001, 90, 644-649.	2.5	3

#	Article	IF	CITATIONS
109	Observation of anomalous phonons in orthorhombic rare-earth manganites. Applied Physics Letters, 2010, 97, 262905.	3.3	3
110	A New Intermetallic NiSn ₅ Phase: Induced Synthesis, Crystal Structure Resolution, and Investigation of Its Mechanism. Journal of Physical Chemistry Letters, 2019, 10, 2561-2566.	4.6	3
111	Synthesis and Processing by Design of Highâ€Nickel Cathode Materials. Batteries and Supercaps, 2022, 5, .	4.7	3
112	Depth-dependent critical behavior in <mml:math <br="" xmlns:mml="http://www.w3.org/1998/Math/MathML">display="inline"><mml:mrow><mml:msub><mml:mtext>V</mml:mtext><mml:mn>2</mml:mn></mml:msub><m Physical Review B, 2009, 79, .</m </mml:mrow></mml:math>	1111 managements	•H2/mml:mte
113	Kinetic Limitations in Singleâ€Crystal Highâ€Nickel Cathodes. Angewandte Chemie, 2021, 133, 17490-17495.	2.0	2
114	Monte Carlo ray-tracing error analysis of a sagittal-focusing optical system as applied to synchrotron radiation. Review of Scientific Instruments, 2002, 73, 1499-1501.	1.3	1
115	Transmission of x-ray polarization through glass capillary fibers. Review of Scientific Instruments, 2003, 74, 23-27.	1.3	1
116	Interfacial Structures of Polyurethane Thin Films on Various Substrate Materials. Polymer Journal, 2003, 35, 929-937.	2.7	1
117	Direct extraction of quantitative structural information from x-ray fluorescence holograms using spherical-harmonic analysis. Physical Review B, 2012, 85, .	3.2	1
118	Effect of the polyurethane crystalline interphase formed at an Al surface on water-vapor absorption. Journal of Applied Polymer Science, 2003, 89, 1417-1422.	2.6	0
119	X-ray characterization of atomic-layer superlattices. Journal Physics D: Applied Physics, 2005, 38, A147-A153.	2.8	0
120	Scaled Up Pulsed Deposition Technology: Carburization Resistant Ablation Coatings for Ethylene Pyrolysis Coils. Materials Research Society Symposia Proceedings, 2005, 890, 1.	0.1	0
121	Mechanisms for species-selective oriented crystal growth at organic templates. Journal of Materials Research, 2007, 22, 2785-2790.	2.6	0
122	Rate-dependent Reversal of Lithium Concentration During Intercalation into LixFePO4 Nanoparticles. Microscopy and Microanalysis, 2018, 24, 1482-1483.	0.4	0
123	Multimodal Analysis of Reaction Pathways of Cathode Materials for Lithium Ion Batteries. Microscopy and Microanalysis, 2020, 26, 906-908.	0.4	0